J. Fluid Mech. (1991), *vol.* 232, *pp.* 377–402
Printed in Great Britain

A turbulent flow over a curved hill. Part 2. Effects of streamline curvature and streamwise pressure gradient

By V. BASKARAN†, A. J. SMITS‡ AND P. N. JOUBERT
Department of Mechanical Engineering, University of Melbourne, Parkville 3052, Australia

(Received 7 February 1990 and in revised form 8 April 1991)

The changes in turbulence in a flow over a two-dimensional curved hill, described in Part 1 (Baskaran, Smits & Joubert 1987), are analysed in the light of transport equations for the turbulent kinetic energy, $\frac{1}{2}\overline{q^2}$, and the primary shear stress, $-\overline{uv}$, in order to infer the way in which the extra strain rates due to streamline curvature and the streamwise pressure gradient contribute to the changes. Interaction between the two extra strain rates is also considered. The triple correlation data presented here are consistent with the fact already established in Part 1 that the upwind boundary-layer structure bifurcates to form two distinct turbulent zones over the hill, namely, an internal boundary layer and an external free turbulent flow. The source terms in the transport equations imply that the effects of streamline curvature and streamwise pressure gradient are felt differently on $\overline{q^2}$ and $-\overline{uv}$. The present experimental results show that the shear stress is more sensitive to streamline curvature than is the turbulent kinetic energy. The anisotropy parameter, $\overline{u^2}/\overline{v^2}$, plays a major role in determining the difference in the behaviour of $\overline{q^2}$ and $-\overline{uv}$ under the influence of streamline curvature. The distribution of turbulent lengthscales follows the general formulae suggested by Bradshaw (1969) for streamline curvature of either sign. The pressure–strain redistribution term deduced from the experimental data is in good agreement with the model of Zeman & Jensen (1987) for flows over hills. The influence of streamwise pressure gradient enters through the normal stress production terms, which appears only in the transport equation for $\overline{q^2}$. The transport terms are found to be affected by streamline curvature. To the thin shear layer approximation, the interaction between streamline curvature and streamwise pressure gradient appears to be weak.

1. Introduction

The present paper is a part of a long-term study on the behaviour of turbulent boundary layers under the influence of longitudinal streamline curvature and streamwise pressure gradient, and specifically it is a sequel to the study reported by Baskaran, Smits & Joubert (1987) (hereinafter referred to as BSJ1) on a turbulent flow over a curved hill. The flow suffered successive changes in pressure gradient and streamline curvature, both alternating in sign: the pressure gradient changed from adverse to favourable and to adverse, and the curvature changed from flat to concave and then to convex. The flow over the convex surface eventually separated. In BSJ1, it was demonstrated that an internal boundary layer developed over the

† Aeronautical Research laboratory, DSTO Salisbury, Australia.
‡ Department of Mechanical and Aerospace Engineering, Princeton University, NJ 08544, USA.

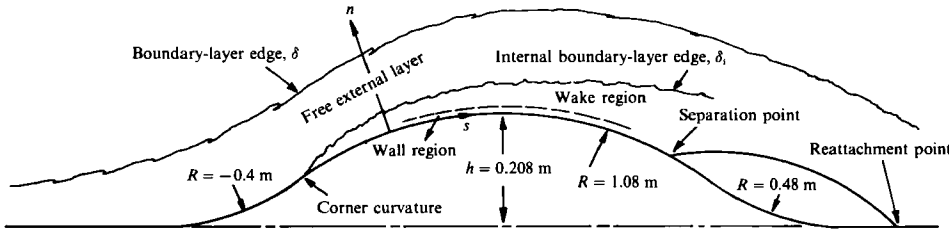

FIGURE 1. The turbulent flow over the curved hill.

convex surface. This internal layer grew much like a sub-boundary layer beneath a free external layer, and as it developed it established its own wall (inner) and wake (outer) regions, as depicted in figure 1. Some of the results presented in BSJ1 indicated that a bifurcation† occurred in the boundary-layer structure near the corner curvature (concave to convex), and the subsequent development of the internal and external layers seemed to take place virtually independently. The perturbation responsible for triggering the internal boundary layer was shown to be the step change in wall curvature rather than the step change in streamwise pressure gradient that occurs at the middle of the concave bend (adverse to favourable). The mean vorticity and total pressure at the wall necessarily change under both types of perturbation (Morton 1984), and the changes near the corner curvature are not consistent with that expected of a streamwise pressure gradient. For example, the turbulent normal stresses were found to change all across the layer rather than simply in the inner region of the boundary layer. In BSJ1, it was also shown that the effect of step change in wall curvature was different from that due to streamline curvature, and the need to distinguish the two effects was stressed, especially in *strongly* curved flows. The present paper deals with the latter effect (streamline curvature) on the various regions on the curved hill, namely the concave bend (including the exit region where the streamline curvature is inflexional), and the internal and external layers. The effect of streamwise pressure gradient on these regions is also considered alongside streamline curvature in order to infer any possible interaction between the two effects.

The behaviour of turbulent flows under the influence of longitudinal streamline curvature has been the subject of intensive experimental research especially over the past two decades, with the common aim of improving turbulence modelling algorithms. Most of the earlier experiments and calculation methods on curved turbulent flows were reviewed by Gillis & Johnston (1983), who studied the response of turbulent boundary layers to the introduction and removal of convex curvature for two cases of $\delta_0/R = 0.05$ and 0.1‡ (δ_0 is the boundary-layer thickness at the start of curvature and R is the radius of curvature of the surface). They reported the formation of two regions over the convex region, namely a slowly developing 'active shear stress layer' and an isolated region above the shear stress layer, which merely conveyed the 'debris' of the upstream boundary layer. Turbulence in the isolated

† We mean by bifurcation, formation of two distinct turbulent zones over the hill. The behaviour of normal stresses at the exit region (figure 14 of BSJ1) of the hill imply a change in the species of large-scale structure.

‡ As shown in BSJ1, δ_0/R does not genuinely represent the effect of streamline curvature, whenever the wall curvature perturbation parameter, $\Delta k^* (= \nu \Delta k/U_{\tau_0})$, exceeds certain threshold limit. Here we use δ_0/R merely to refer to earlier experiments as 'mild' and 'strong' cases following convention.

region was shown to be 'isotropic'. The main effect of convex curvature was found to be a reduction in the turbulence lengthscales.

A similar study by Prabhu & Sundarasiva Rao (1981) used δ_0/R, namely 0.038, 0.068 and 0.144. Both concave and convex curvature were investigated. In the convex case, the results indicated a decoupling of the inner ($n/\delta < 0.2$) and outer regions of the boundary layer, and the shear stress over the curved region was found to be insensitive to variations in δ_0/R. Taylor–Görtler roll cells were detected over the concave surface for all cases investigated. Measurements in a turbulent boundary layer over a convex surface with a much smaller value of δ_0/R (0.01) were reported by Gibson, Verriopoulos & Vlachos (1984) and Gibson & Verriopoulos (1984), who studied aspects of both momentum transfer and heat transfer. The turbulent stresses and the triple velocity correlations were found to decrease under the influence of convex curvature, and the Reynolds heat flux was found to be more sensitive than the Reynolds shear stress to changes in wall curvature. In related experiments by Muck, Hoffmann & Bradshaw (1985) and Hoffmann, Muck & Bradshaw (1985), measurements over convex and concave surfaces were made using the same ratio of δ_0/R as in the experiments of Gibson *et al.* The response of the turbulent boundary layer to convex and concave curvature was found to be totally different even qualitatively, with convex curvature affecting the structure faster than the concave curvature. For example, the response to the introduction of convex curvature was found to be less than $5\delta_0$ (Gillis & Johnston 1983), while in the concave case of Barlow & Johnston (1988), the response was found to be more than $10\delta_0$. The general behaviour under mild conditions (with small δ_0/R) was found to be grossly different from that under strong conditions, and in BSJ1, we attempted to explain this observation by using the concept of internal boundary layers and the perturbation caused by a step change in wall curvature.

The experiments on the effect of streamline curvature on free turbulent flows such as mixing layers, jets and wakes are few in number in comparison with that on boundary layers. Measurements in a curved mixing layer were reported by Castro & Bradshaw (1976), where a fully developed plane mixing layer experienced the effects of stabilizing curvature before relaxing back to the plane conditions. The Reynolds stresses, after an initial decrease in the curved region owing to the stabilizing effect, were found to overshoot the plane-layer values before recovering to their original levels. Koyama (1983) made measurements in a developing curved wake of a circular cylinder, and Savill (1983) studied the structure of a curved circular cylinder wake turning through 90°. The Reynolds stresses were suppressed completely on the stable side by the time the wake had turned through 20° and the structure on the unstable side expanded onto the stable side. Nakayama (1987) reported measurements in a self-preserving small defect wake from a circular cylinder which experienced the effects of both streamline curvature and streamwise pressure gradients. The extra strain rates overwhelmed the basic shear, and as a consequence even the 'fairly thin-shear-layer' approximation was violated. [A shear layer in which the ratio of the extra strain rate to the basic shear satisfies the inequality, $e/(\partial U/\partial n) < 0.1$, but need not satisfy the 'thin-shear-layer or boundary-layer approximation inequality', $e/(\partial \mathrm{U}/\partial n) \ll 1$, is classified as a 'fairly thin shear layer' (Bradshaw 1973).] The ratios of the extra strain rate to basic shear due to pressure gradient were about 0.2, while those due to streamline curvature attained values as large as -0.5. Owing to this, the interaction between the two extra strain rates could not be inferred clearly. More recently, Ramjee, Tulapurkara & Rajasekar (1988) made measurements in a curved wake downstream of a symmetric airfoil and found an asymmetric mean velocity

distribution across the wake. Turbulence was found to be amplified on the unstable side, while it was suppressed on the stable side.

The relation between the present case and meteorological hill flows was discussed in BSJ1, where the results were compared with the theoretical predictions of Jackson & Hunt (1975). The theory qualitatively reproduced the changes observed in the inner region where the perturbations due to pressure gradients were strong, even though the limitations set by the theory were severely violated. For example, the slenderness ratio (height/length) of the present hill was much larger than the Gaussian hill assumed in theory and the ratio of the inner region of the upwind boundary layer to the height of the hill was much smaller. In addition, the effect of streamline curvature on the hill flow behaviour was altogether neglected in the theory. More recently, Zeman & Jensen (1987) successfully modelled the turbulent flow behaviour over a Gaussian hill, but found that streamline curvature played a major role outside the inner region. The terms in the transport equations for the turbulent kinetic energy and the shear stress were modelled individually. In particular, the curvature contribution to the pressure–strain redistribution term was introduced in their model explicitly, apart from the usual rapid distortion and return-to-isotropy contributions. Since the changes (decrease of all Reynolds stresses) in the outer region of the internal boundary layer were consistent with that expected of convex streamline curvature (figure 29 of BSJ1), we have compared this model with the present results. Except for the concave bend, surprisingly good agreement is found.

2. Effects of streamline curvature and streamwise pressure gradient

The results to be presented in this paper are discussed in the light of the transport equations for the turbulent kinetic energy, $\frac{1}{2}\overline{q^2}$, where $\overline{q^2}\,(=\overline{u^2}+\overline{v^2}+\overline{w^2})$, and the primary shear stress, $-\overline{uv}$, as these equations are widely used as the basis in the development of many engineering calculation methods. The transport equations for these two quantities in a curvilinear coordinate system (figure 1) are (Bradshaw 1973; Castro & Bradshaw 1976).

$$\underbrace{\left[U\frac{\partial}{\partial s}+\left(1+\frac{n}{R}\right)V\frac{\partial}{\partial n}\right](\tfrac{1}{2}\overline{q^2})}_{\text{advection}}=\underbrace{-\overline{uv}\left(1+\frac{n}{R}\right)\frac{\partial U}{\partial n}}_{\text{shear production}}\underbrace{-(\overline{u^2}-\overline{v^2})\left[\frac{\partial U}{\partial s}+\frac{V}{R}\right]}_{\text{normal stress production}}$$

$$\underbrace{-\overline{uv}\left[\frac{\partial V}{\partial s}-\frac{U}{R}\right]}_{\text{curvature production}}\underbrace{-\frac{\partial}{\partial s}\left(\frac{\overline{pu}}{\rho}+\tfrac{1}{2}\overline{q^2u}\right)-\frac{\partial}{\partial n}\left[\left(1+\frac{n}{R}\right)\left(\frac{\overline{pv}}{\rho}+\tfrac{1}{2}\overline{q^2v}\right)\right]}_{\text{pressure cum turbulent diffusion}}\underbrace{-\epsilon}_{\text{dissipation}},\quad(1)$$

$$\underbrace{\left[U\frac{\partial}{\partial s}+\left(1+\frac{n}{R}\right)V\frac{\partial}{\partial n}\right](-\overline{uv})}_{\text{mean transport}}=\underbrace{\overline{v^2}\left(1+\frac{n}{R}\right)\frac{\partial U}{\partial n}}_{\text{shear generation}}+\underbrace{\overline{u^2}\left(\frac{\partial V}{\partial s}-\frac{U}{R}\right)}_{\text{curvature generation}}\underbrace{-(\overline{u^2}-\overline{v^2})\frac{U}{R}}_{\text{coordinate rotation}}$$

$$\underbrace{+\frac{\partial}{\partial s}\left(\frac{\overline{pv}}{\rho}+\overline{u^2v}\right)+\frac{\partial}{\partial n}\left[\left(1+\frac{n}{R}\right)\left(\frac{\overline{pu}}{\rho}+\overline{uv^2}\right)\right]+\left(\frac{\overline{uv^2}-\overline{u^3}}{R}\right)}_{\text{pressure cum turbulent transport}}\underbrace{-\overline{\frac{p}{\rho}\left[\frac{\partial v}{\partial s}+\left(1+\frac{n}{R}\right)\frac{\partial u}{\partial n}\right]}}_{\text{pressure–strain redistribution}}.\quad(2)$$

We have chosen the (s, n, z) curvilinear coordinate system fixed to the surface (figure 1) for analysis because the measurements were made in accordance with this system. The system is also preferable for the calculation of the flow with geometry such as the present one. Here, we retain all the terms that arise owing to both streamline curvature and coordinate transformation from the Cartesian (x, y, z) coordinate system.

The terms in both equations have been given their usual names, except that the production and generation terms have been split into three separate parts to help identify their origin. The extra strain rates due to streamline curvature and streamwise pressure gradient in the present coordinate system are $[(\partial V/\partial s)-(U/R)]$ and $[(\partial U/\partial s)+(V/R)]$ respectively. Note that the pseudogeneration term in (2), $(\overline{u^2}-\overline{v^2})(U/R)$, represents the contribution due to the rotation of axes, and hence is not due to streamline curvature. This term is usually small since streamlines cannot change direction abruptly, even though it tends to reduce the overall production unless $\overline{v^2} > \overline{u^2}$. The rotation term is normally absorbed into the curvature generation term (see for example, Zeman & Jensen 1987). In the above equations we have retained the terms involving V as we are not applying these equations strictly along streamlines, nor could we assume implicitly, as in many other curved flow investigations, that the streamlines are parallel to the profile of the hill. In fact, the static pressure measurements across the boundary layer presented in BSJ1 indicated that the streamlines were not parallel to the surface, especially in the regions of strong acceleration (concave bend and exit regions) and strong retardation (before separation point).

There is no contribution to the shear stress generation from the extra strain rate due to pressure gradient in (2). The absence of the extra strain rate due to pressure gradient elsewhere in (2) suggests that the shear stress is not affected directly. If the mean momentum equation is used to form an equation for $\partial U/\partial n$, it can be shown that away from the wall where viscous effects are small (outer region), $\partial U/\partial n$ cannot respond to changes in streamwise pressure gradient (Bradshaw & Ferris 1965). Since the primary production and generation terms in (1) and (2) contain $\partial U/\partial n$, it follows that a sudden change in pressure gradient cannot also produce a change in $\overline{q^2}$ and $-\overline{uv}$, except as far as the normal stress production term in (1) becomes important. It should be noted that by using the continuity equation the normal stress production can be written as $(\overline{u^2}-\overline{v^2})(1+n/R)\,\partial V/\partial n$, and the effect of the streamwise pressure gradient can also be interpreted in terms of $\partial V/\partial n$. The effect of $\partial V/\partial n$ is reported to be insignificant on boundary layers (Bradshaw 1973) even though its sign in free turbulent flows, according to Townsend (1961), distinguishes wakes and jets.

The production terms in (1) and the generation terms in (2) are of the form (turbulent stress × rate of strain of mean flow). The ratio of curvature production to shear production in (1) is normally used as a measure of streamline curvature effect as it gives the ratio of the extra strain rate to the simple shear. When this measure is applied to the generation terms in (2), it shows that the generation of $-\overline{uv}$ depends not only on the ratio of strain rates, but also on the anisotropy parameter, namely $\overline{u^2}/\overline{v^2}$ (see Hunt & Joubert 1979). Therefore, the behaviour of $\overline{q^2}$ is expected to be different from that of $-\overline{uv}$ in a curved flow as far as $\overline{u^2} \neq \overline{v^2}$. Similarly, the effect of streamwise pressure gradient on $\overline{q^2}$ in addition to the ratio of strain rates depends on the above ratio of the normal stresses as well as the shear stress covariance, $\overline{v^2}/-\overline{uv}$. An alternative interpretation of the generation terms in (2) is achieved by rearranging the terms such that the leading-order contribution to the generation is proportional to the basic strain, $(\partial U/\partial n)-(U/R)$. By using R_c, the ratio of the extra strain rate

$2U/R$ to the basic strain, this term becomes $(\overline{v^2}(1+R_c)-\overline{u^2}R_c)[(\partial U/\partial n)-(U/R)]$, which again demonstrates the important role of the anisotropy parameter in determining the effects of curvature.

Gibson & Rodi (1981) used a full Reynolds stress model based on (2) to calculate the curved mixing-layer flow studied by Castro & Bradshaw (1976), and found good agreement between experiment and calculation without modification to the basic closure hypotheses, and without changes in the basic constants. On the other hand, lower-order models, such as the one-equation model due to Bradshaw & Unsworth (1974), certainly require empirical curvature corrections to obtain reasonable agreement with experiment. For even a small extra strain rate, the changes in the Reynolds stresses was found to be an order of magnitude larger than the ratio of the extra strain rate to the mean shear. Most of the changes due to extra strain rates arise in terms which do not contain the extra strain rates explicitly, such as the diffusion and destruction terms. Gibson & Rodi emphasized that the correct modelling of the pressure–strain correlation was particularly important for the success of their calculation. Muck *et al.* (1985) added, 'it may be advisable to model the effects of curvature solely in the Reynolds stress equations, at least partly as a dependence of the *rapid* part of the pressure–strain redistribution term in the Reynolds stress transport equation on a suitable dimensionless curvature parameter'. The model of Zeman & Jensen (1987), used to compare the present experimental results essentially incorporates such a mechanism, and their model for the full pressure–strain redistribution term is,

$$\Pi^{uv} = \underbrace{-0.6\overline{v^2}\frac{\partial U}{\partial n}}_{\text{rapid part}} + \underbrace{0.3(2\overline{u^2}-\overline{v^2})\frac{U}{R}}_{\text{curvature part}} \underbrace{-3.25\epsilon\left(\frac{\overline{u^2}}{\overline{q^2}}-\frac{1}{3}\right)}_{\text{return-to-isotropy part}} \tag{3}$$

3. Results and discussion

Before discussing the results, the non-dimensionalization of flow variables needs some comment. All the velocities and the lengths are non-dimensionalized with respect to some fixed values, namely the reference velocity, U_{ref}, and δ_0, the boundary-layer thickness at the first measurement station ($s = 596$ mm), in order to observe the absolute changes due to streamline curvature and streamwise pressure gradient. Scaling with the local values such as the wall potential velocity, U_{pw}, and the local boundary-layer thickness, δ, has the disadvantage of disguising the effects of the extra strain rates and may mislead interpretation. It is not our intention to derive any similarity laws in the present work.

The profiles of $\overline{q^2}$ and $-\overline{uv}$ over the curved hill are shown in figure 2. The profiles of $\overline{q^2}$ over the leading-edge plate ($s < 897$ mm) exhibit relatively little change. $\overline{q^2}$ increases to the concave bend only below $n/\delta = 0.5$, against the expected increase due to the destabilizing curvature at a larger distance from the wall. At the exit, where the streamline curvature is inflexional, $\overline{q^2}$ decreases to a level comparable to values over the leading-edge plate. The behaviour of turbulent kinetic energy over the prolonged region of convex curvature is closely similar to that of the individual normal stresses. Inside the internal boundary layer over the hill, all the stresses increase with downstream distance in the inner or wall region (figure 1), while they decrease in the outer region (refer to figure 29 in BSJ1). Unlike in the *strongly* curved

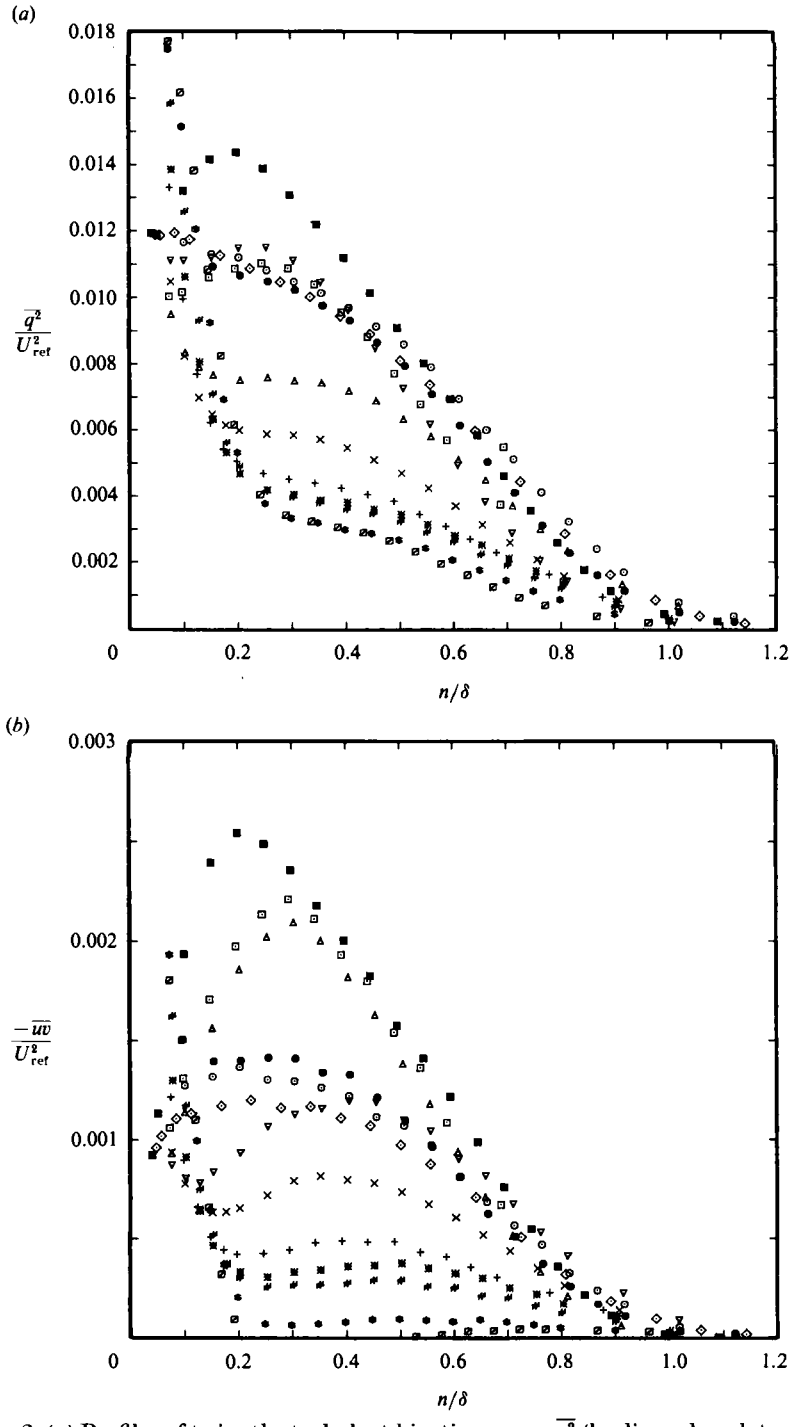

FIGURE 2. (*a*) Profiles of twice the turbulent kinetic energy, $\overline{q^2}$ (leading-edge plate: ●, $s = 596$ mm; ⊙, 710; ◇, 897 (foot of the hill); concave bend: ■, 1015; exit: ⊡, 1139; ▽, 1183; convex curvature: △, 1345; ×, 1469; +, 1596; ✱, 1665; ✱, 1730; ⬢, 1862; ∅, 1990). (*b*) Profiles of primary shear stress, $-\overline{uv}$. △, 1183 mm; ▽, 1345 (symbols for other stations same as in figure 2(*a*)).

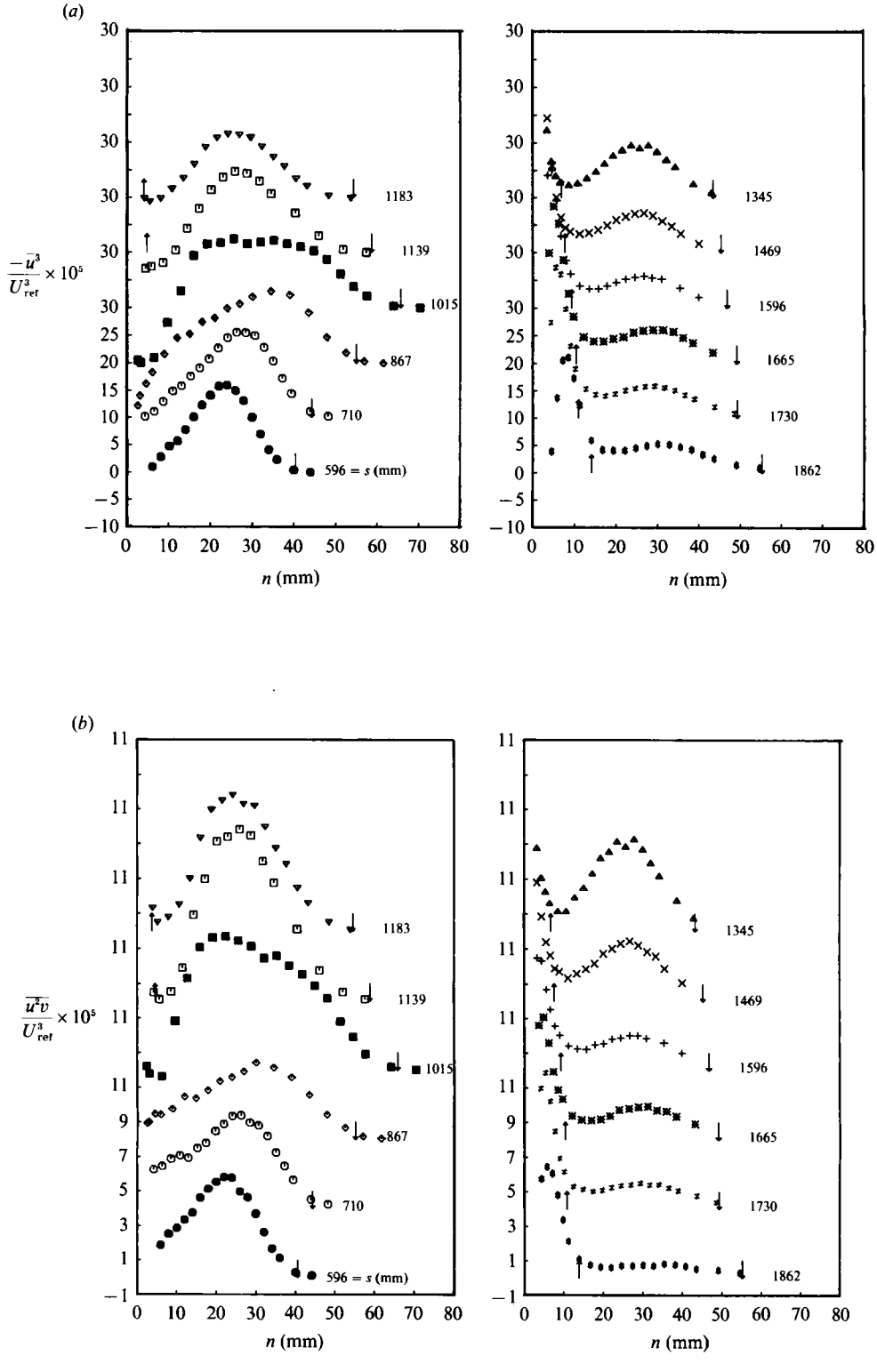

FIGURE 3(a, b). For caption see page 387.

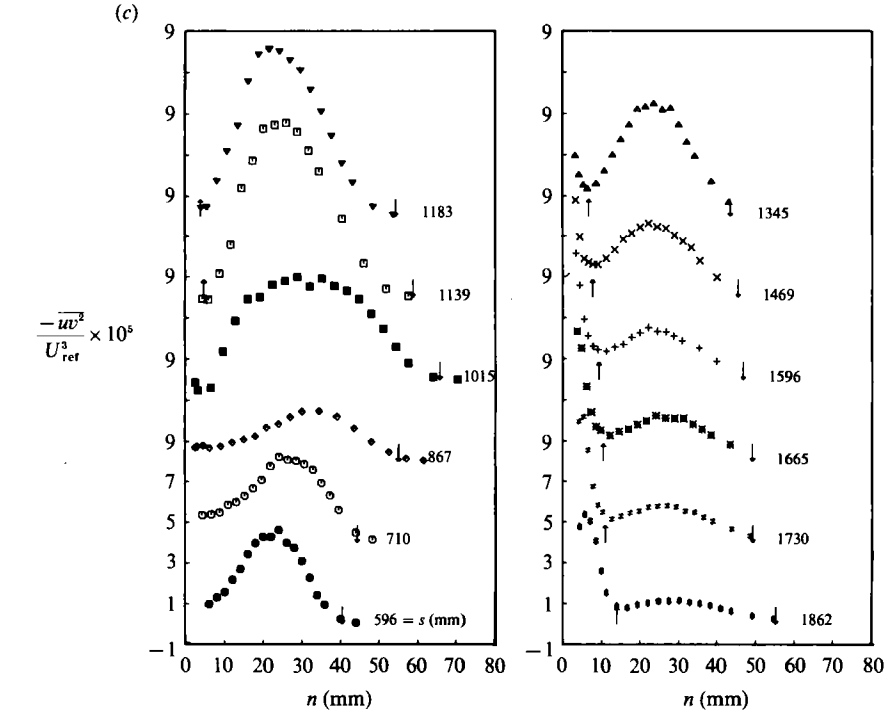

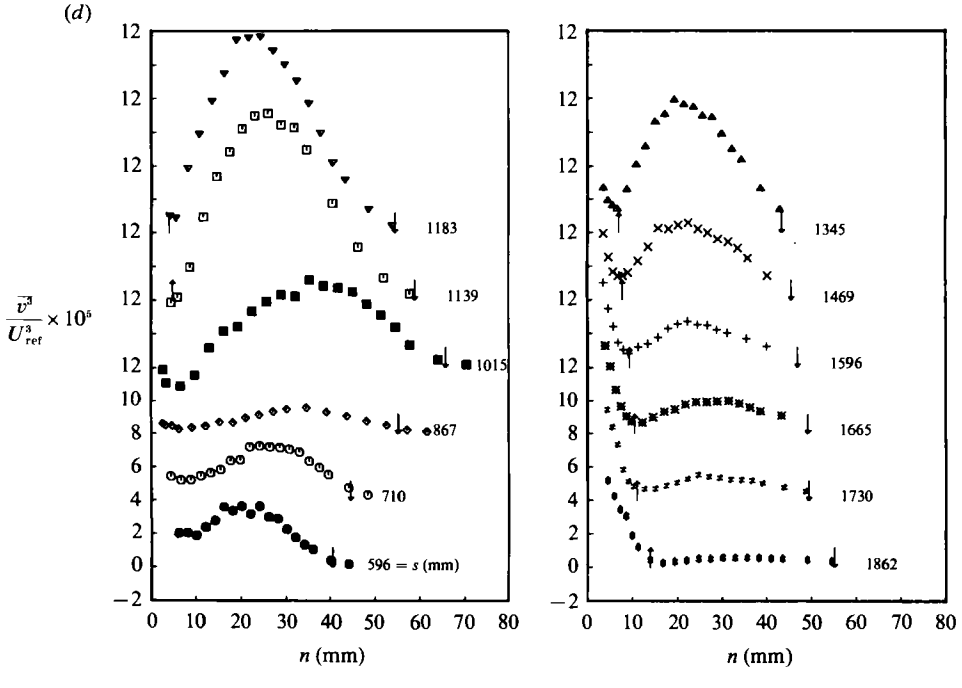

FIGURE 3 (*c*, *d*). For caption see page 387.

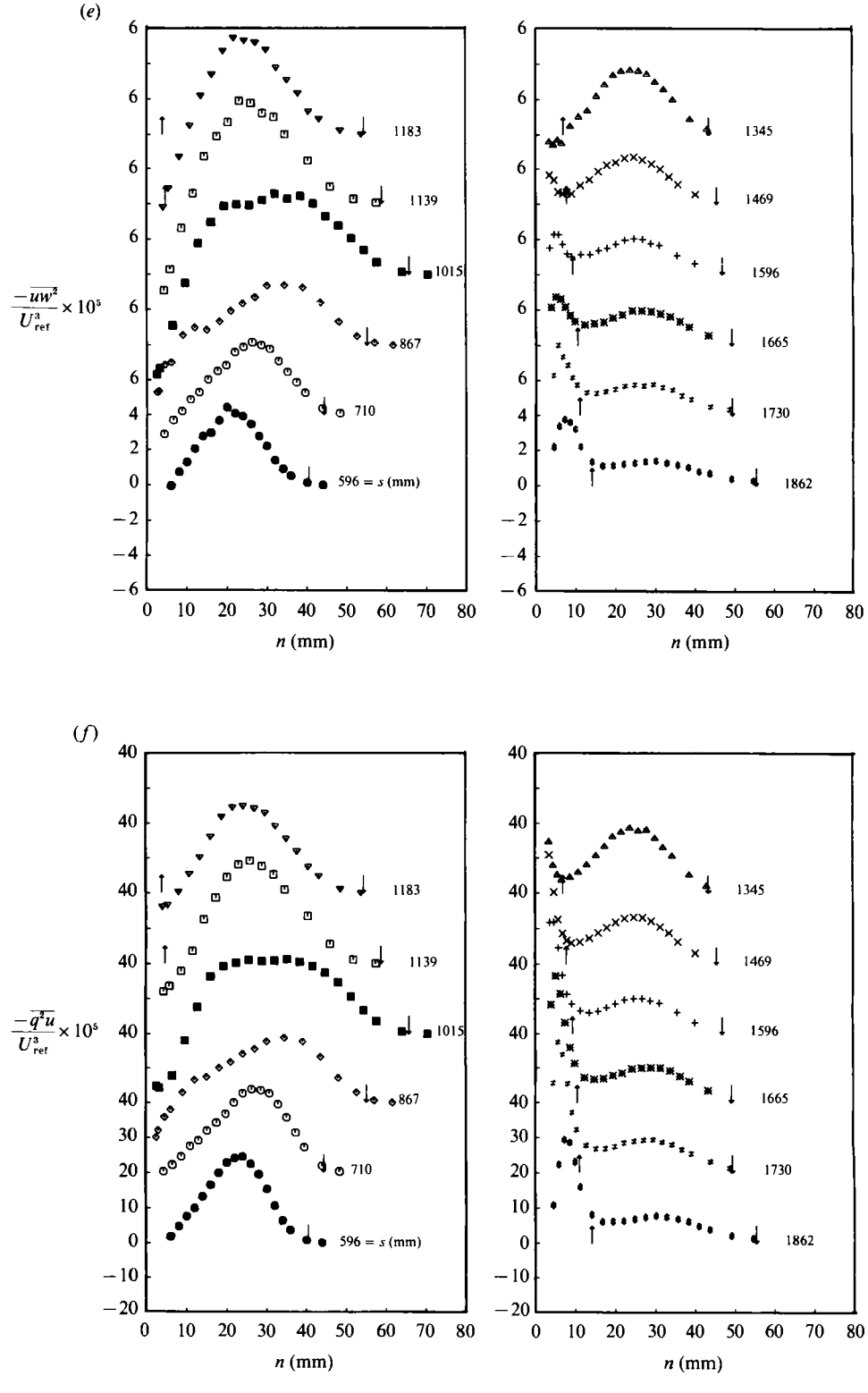

FIGURE 3(e,f). For caption see facing page.

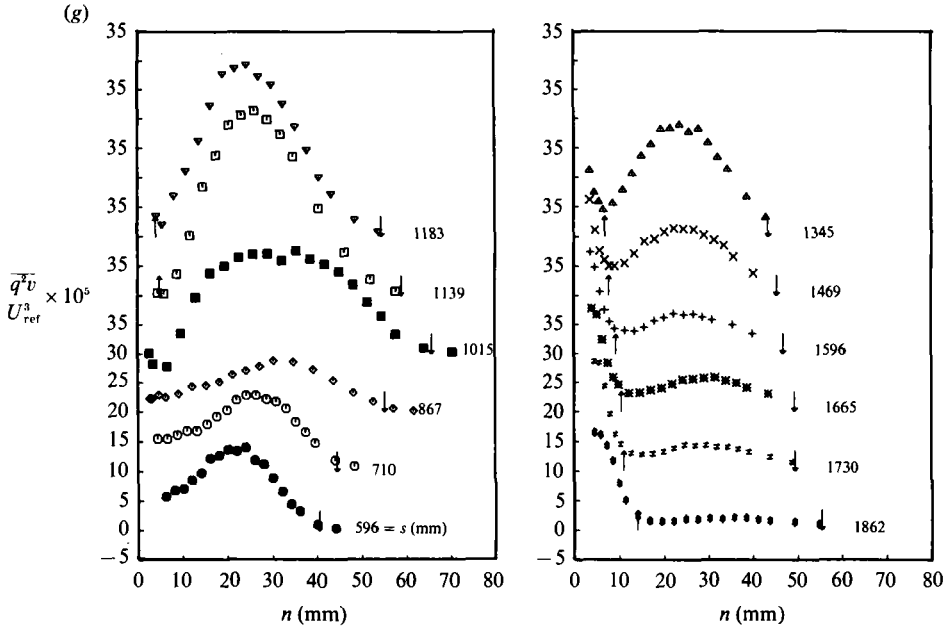

FIGURE 3. Profiles of triple products. (*a*) $-\overline{u^3}/U^3_{ref}$; (*b*) $\overline{u^2v}/U^3_{ref}$; (*c*) $-\overline{uv^2}/U^3_{ref}$; (*d*) $\overline{v^3}/U^3_{ref}$; (*e*) $-\overline{uw^2}/U^3_{ref}$; (*f*) $-\overline{q^2u}/U^3_{ref}$; (*g*) $\overline{q^2v}/U^3_{ref}$. ↑, δ_i; ↓, δ. (For legend refer to figure 2(*a*) and note shift in ordinate scale.)

flows studied by earlier workers such as So & Mellor (1972), Prabhu & Sundarasiva Rao (1981) and Gillis & Johnston (1983), the stresses in the external layer decrease only gradually with streamwise distance since there is an increase in their magnitudes in the concave bend. The profiles of $-\overline{uv}$ demonstrate that shear stress decreases faster than the turbulent kinetic energy over the convex region especially in the external layer (see BSJ1 for a fuller discussion of the shear stress profiles). At the last measurement station before the separation point, the shear stress even changes sign between $n/\delta = 0.2$ and $n/\delta = 0.5$ (negative values are not shown).

The triple products of velocity fluctuations, namely $\overline{u^3}$, $\overline{u^2v}$, $\overline{uv^2}$, $\overline{v^3}$, $\overline{uw^2}$, $\overline{q^2u}$ $(=\overline{u^3}+\overline{uv^2}+\overline{uw^2})$ and $\overline{q^2v}$ $(=\overline{u^2v}+\overline{v^3}+\overline{w^2v})$ are shown in figure 3. The quantity, $\overline{vw^2}$ was inferred to be $\frac{1}{2}(\overline{u^2v}+\overline{v^3})$ following Bradshaw (1967). Details of the measurement techniques were already discussed in BSJ1 and will not be repeated here. The pressure–velocity correlations contained in (1) and (2) could not be measured. Dissipation in (1) and redistribution in (2) including the terms containing pressure fluctuations were obtained as the sum of other terms.

The triple products increase significantly through the concave bend before encountering convex curvature, and therefore turbulent diffusion of $\overline{q^2}$ and turbulent transport of $-\overline{uv}$ are expected to be affected. The behaviour of the triple products over the convex surface clearly supports the existence of the internal and external layers over the hill through the presence of the knee points as already observed in the profiles of the Reynolds normal and shear stresses in BSJ1. Within the internal boundary layer, the triple products maintain levels typical of the upstream boundary layer, whereas in the external layer the triple products monotonically attenuate to very low levels. The thickness of the internal layer, δ_i, and the external layer, $\delta_e(=\delta-\delta_i)$, along with other flow parameters, which describe and govern the flow over the two-dimensional hill, are given in table 1. Note that the width of the

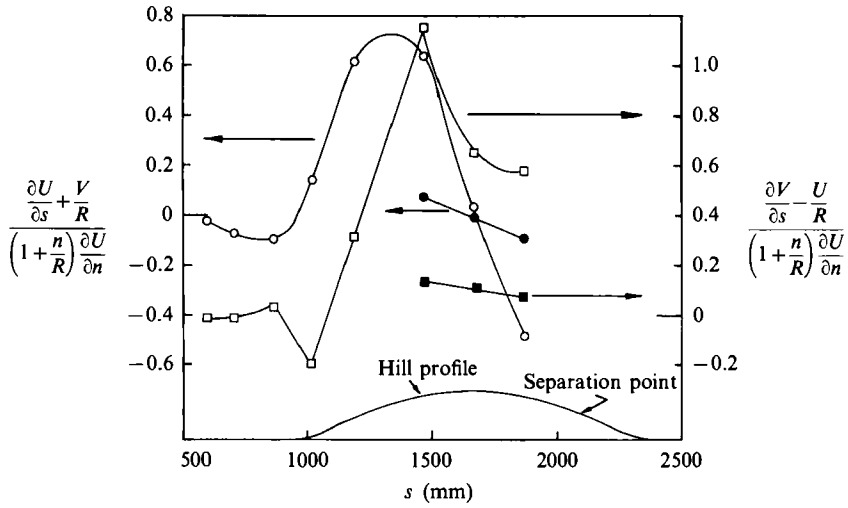

FIGURE 4. Ratio of extra strain rates to simple shear. ○. Streamwise pressure gradient, $[(\partial U/\partial s)+(V/R)]/[1+(n/R)](\partial U/\partial n)$; □, streamline curvature, $[(\partial V/\partial s)-(U/R)]/[1+(n/R)](\partial U/\partial n)$. (Open symbols refer to $n/\delta = 0.5$; solid symbols refer to $n/\delta_i = 1$.)

s (mm)	C_{pw}	$C_f \times 10^3$	$K \times 10^6$	δ (mm)	δ_i (mm)	δ_e (mm)
596	0.097	2.96	−0.16	39.19	—	—
710	0.148	2.81	−0.27	43.08	—	—
867	0.285	2.06	−0.86	53.83	—	—
1015	0.364	2.41	0.65	64.54	—	—
1139	0.001	4.76	1.77	52.85	3.43	49.42
1183	−0.177	5.08	1.25	53.12	2.66	47.46
1345	−0.726	4.77	0.44	42.15	5.48	36.67
1469	−1.014	4.28	0.28	44.08	6.39	37.69
1596	−1.252	3.88	0.18	45.53	7.97	37.56
1665	−1.132	3.29	0.05	47.93	9.11	38.82
1730	−1.267	3.54	−0.19	48.09	9.62	38.47
1862	−0.995	2.69	−0.30	54.03	12.7	41.33
1990	−0.579	1.35	−0.77	70.52	17.28	53.24

TABLE 1. Flow parameters for the turbulent flow over the curved hill. $U_{ref} = 20.6 \pm 0.2$ m/s, $\nu = 15.1 \pm 0.1 \times 10^6$ m^2/s. K is a pressure gradient parameter $(= -(\nu/\rho U_{pw}^3)\mathrm{d}p/\mathrm{d}x)$.

free external layer remains more or less constant almost until the region of separation is reached.

In order to assess the significance of the prolonged streamline curvature and the acceleration effects on various regions of the hill, the ratios of the corresponding extra strain rates to the local mean shear are plotted in figure 4 along $n/\delta = 0.5$ and $n/\delta_i = 1$. In the concave bend, the modulus of the ratios of the above two extra strain rates to the local shear reach values as large as 0.2, implying significant changes in the flow owing to the dominance of the Reynolds stress gradients, while at the exit the extra strain rates exceed by far the basic shear, indicating a strong distortion of the turbulence structure. The applicability of even the *fairly thin-shear-layer* approximation is in doubt in these regions. In BSJ1, the behaviour of the normal stresses at the exit of the bend implied a change in the species of the turbulent flow structure, namely from an attached-boundary-layer structure to a free-shear-layer

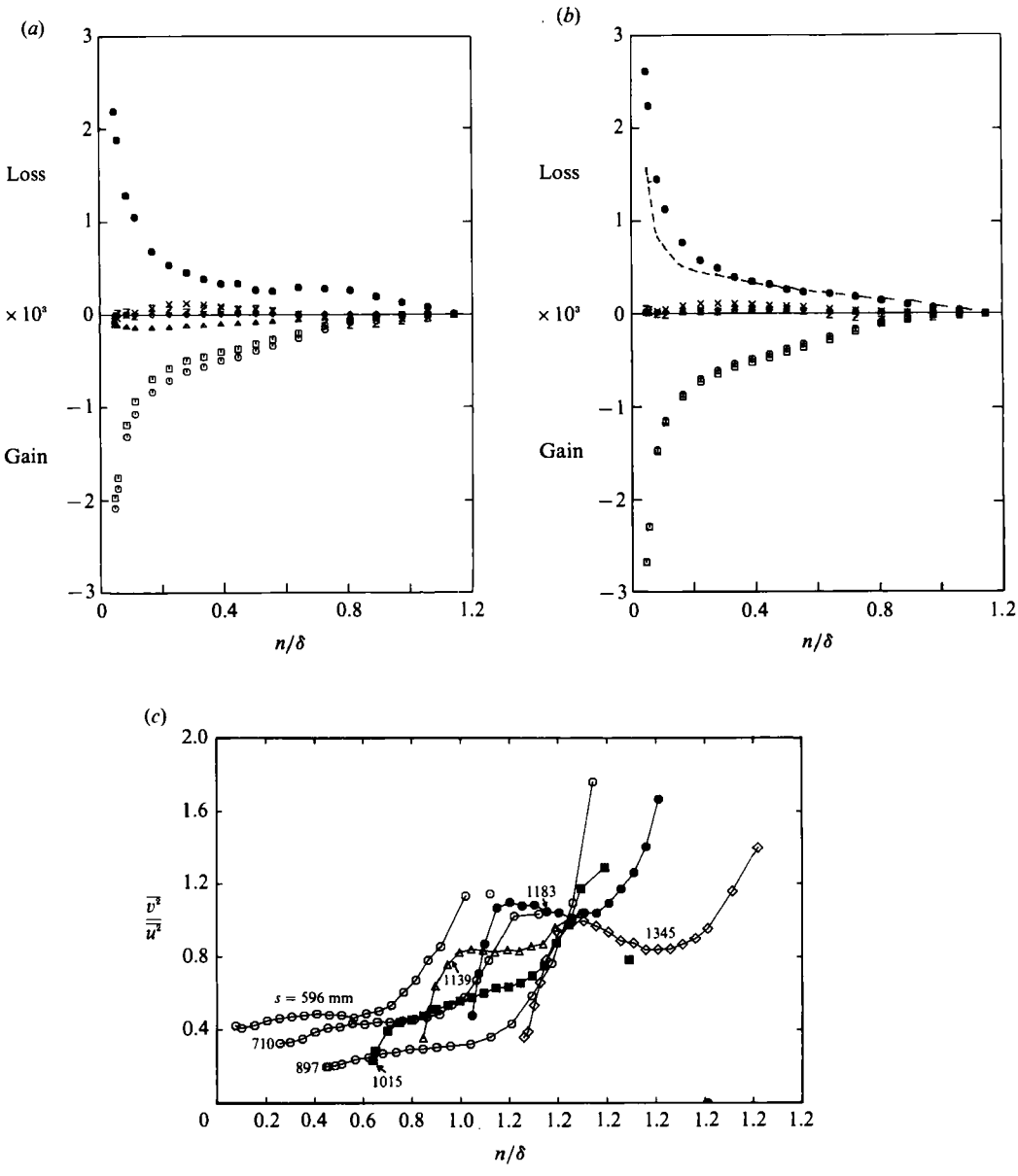

FIGURE 5. (*a*) Turbulent kinetic energy balance at the foot of the hill (s = 897 mm). ×, advection; □, shear production; △, normal stress production; ◇, curvature production; ⊙, total production; Z, turbulent diffusion; ●, dissipation. (Terms non-dimensionalized by δ_0, (δ at s = 596 mm) and $U^3_{\mathrm{ref.}}$.) (*b*) Primary shear stress balance at the foot of the hill (s = 897 mm). ×, mean transport; □, shear generation; ◇, curvature generation; ○, total generation; Z, turbulent transport; ●, pressure–strain redistribution; ---, Zeman & Jenson's model for redistribution. (Terms non-dimensionalized by δ_0 and $U^3_{\mathrm{ref.}}$.) (*c*) Profiles of *anisotropy* parameter, $\overline{v^2}/\overline{u^2}$, around concave bend. (Note the shift in the abscissa scale.)

structure without flow separation. The ratios of the extra strain rates remain high in the isolated external layer, so that the behaviour of the turbulence structure is expected to follow that corresponding to decaying turbulence in a curved path, and one needs to distinguish between the genuine stabilizing curvature effects and the

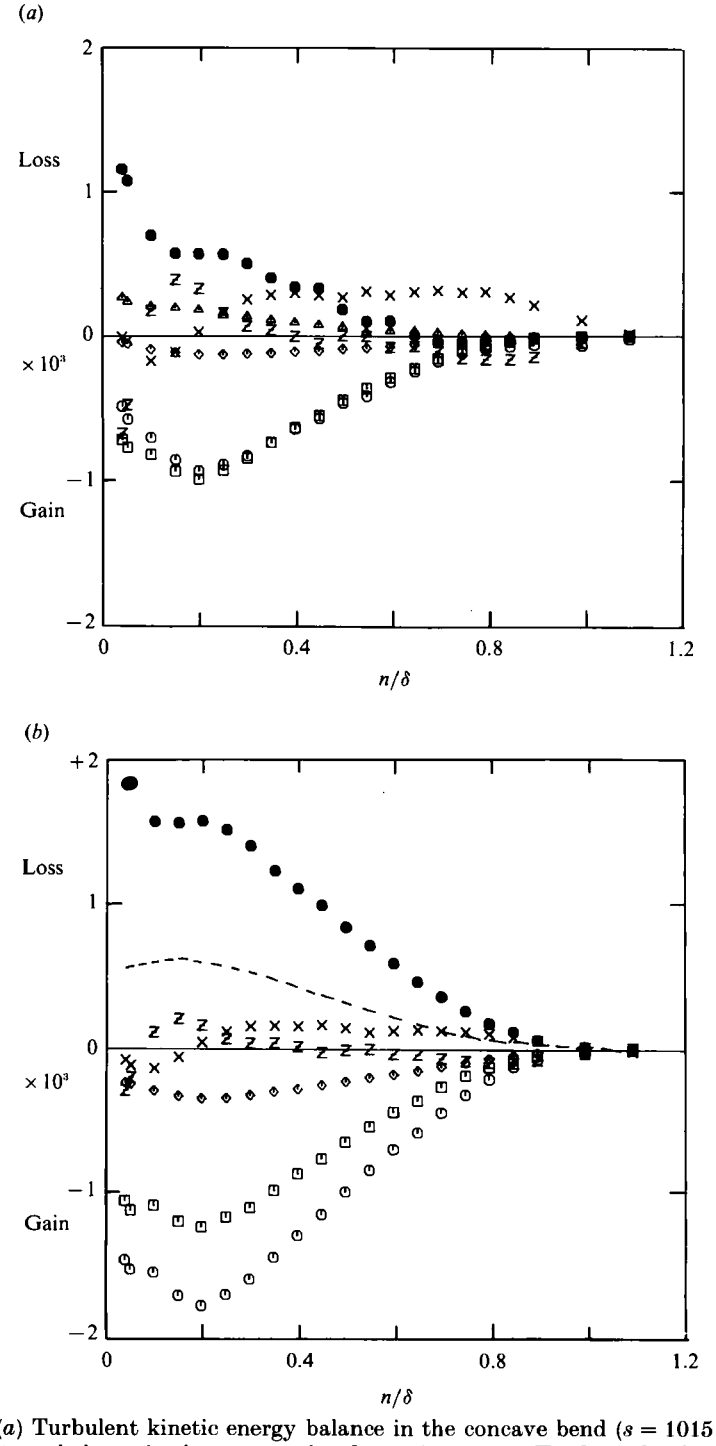

FIGURE 6. (*a*) Turbulent kinetic energy balance in the concave bend (s = 1015 mm). (*b*) Primary shear stress balance in the concave bend (s = 1015 mm). For legend refer to figure 5(*b*).

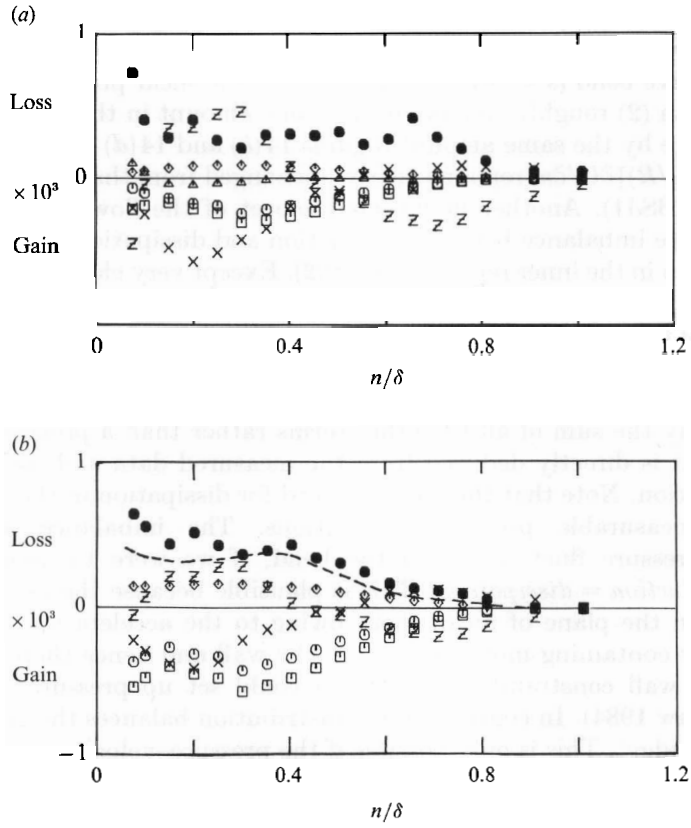

FIGURE 7. (*a*) Turbulent kinetic energy balance at the exit ($s = 1183$ mm). (*b*) Primary shear stress balance at the exit ($s = 1183$ mm). For legend refer to figure 5(*b*).

strong distortion that occurs when the extra strain rate overwhelms the basic shear. When the distortion is that strong, the turbulent stresses change necessarily as a result of direct changes in the inherent large eddy structure (distortion) rather than owing to the extra strain rate itself (Bradshaw 1973). In contrast, the internal boundary layer obeys the thin-shear-layer approximation as the extra strain rates are only about 0.01 of the local shear.

3.1. *Concave bend*

The terms in (1) and (2) in the region of the concave bend, namely at entry ($s =$ 897 mm; also referred to as the foot of the hill), middle ($s = 1015$ mm) and exit ($s =$ 1183 mm) locations are shown in figures 5, 6 and 7 respectively (except figure 5*c*). It is interesting to note that the increase in $\overline{q^2}$ occurs only below $n/\delta = 0.5$ in the concave bend, while the increase in $-\overline{uv}$ occurs all across the layer (figure 2). One would normally expect $\overline{q^2}$ also to increase significantly in the outer region under the influence of concave curvature. Apparently, this is due to the increase due to the curvature production being compensated by a decrease due to the normal stress production, as shown in figure 6(*a*), whereas the shear production increases only slightly between the entry and the concave bend, especially above $n/\delta = 0.2$. In contrast, the gain due to curvature alone on $-\overline{uv}$ generation in the bend is almost as large as the shear generation at the foot of the hill, especially in the outer region ($n/\delta > 0.2$) as shown in figure 5(*b*). This increase in generation is directly due to the

curvature extra strain rate, since the associated anisotropy parameter, $\overline{u^2}/\overline{v^2}$, shown in figure 5(*c*), decreases from a plateau value of 4 at the foot of the hill ($s = 897$ mm) to 2.5 in the concave bend ($s = 1015$ mm). Note that the shear production in (1) and shear generation in (2) roughly change by the same amount in the bend, since both $-\overline{uv}$ and $\overline{v^2}$ change by the same amount (figures 14(*b*) and 14(*d*) in BSJ1) while the basic shear, $[1+(n/R)]\,\partial U/\partial n$, remains nearly unchanged from that at the foot of the hill (figure 24 of BSJ1). Another unexpected aspect of the flow behaviour in the concave bend is the imbalance between production and dissipation of the turbulent kinetic energy even in the inner region ($n/\delta \leqslant 0.2$). Except very close to the wall (first three data points), the dissipation in the bend below $n/\delta = 0.5$ does not change from that at the foot of the hill, while outside this point dissipation decreases to negligibly small values. The excess of advection over diffusion outside $n/\delta = 0.5$ is consistent with the slight decrease in $\overline{q^2}$ in the bend from its value at the foot of the hill. Advection is really the sum of all the other terms rather than a process in its own right. However, it is directly deduced from the measured data and used to derive values for dissipation. Note that the term deduced for dissipation in (1) contains the terms with unmeasurable pressure fluctuations. The imbalance implies the significance of pressure fluctuations in the bend, if we were to assume energy equilibrium (*production = dissipation*). This is plausible because the convergence of the streamlines in the plane of mean shear owing to the acceleration in the bend moves the energy containing motions towards the wall and hence there is likely to be an 'image or wall constraint effect' which could set up pressure fluctuations (Wood & Bradshaw 1984). In contrast, the redistribution balances the generation in the shear stress budget. This is only possible if the pressure–velocity correlation, $\overline{pu}$ is a function of s only and $\overline{pv}$ is a function of n only. It is not possible to check this inference from other experiments on flow through concave bends, such as that by Smits, Young & Bradshaw (1979), since no data were taken in the bend. The model of Zeman & Jensen, while predicting the redistribution at the foot of the hill reasonably well, underestimates the levels in the concave bend by a factor of about 3.

At the exit ($s = 1183$ mm), there is a large reduction in the total production and total generation even though both $\overline{q^2}$ and $-\overline{uv}$ at the exit are quite large; $\overline{q^2}$ recovers almost to the undisturbed values upstream with a slight reduction in the outer layer, and $-\overline{uv}$ remains roughly as high as that in the concave bend with a decrease below $n/\delta = 0.4$. This obviously results in the remaining terms, especially those responsible for diffusion and advection in (1) and mean transport and turbulent transport in (2), becoming at least as large as the source and sink terms. The reduction in total production and total generation is mainly due to significant reduction in the shear production and shear generation terms respectively, and should not be thought to be due to the influence of the streamline curvature, which has just changed sign at the exit. The reduction in shear production and shear generation, in turn is due to the reduction in the basic shear, since $\overline{v^2}$ continues to increase at the exit. Note that the normal stress production in (1) is negligibly small at the exit, even though the extra strain rate due to acceleration is large (0.6) relative to the basic shear strain. This is due to the associated amplification factor, namely $(\overline{u^2}-\overline{v^2})$, being negligibly small. The curvature contribution to both production and generation remains roughly the same as that in the bend, but opposes the shear contribution consistently, as expected of convex curvature. The static pressure distributions across the layer at the exit presented in BSJ1 suggest that the radius of curvature of streamlines is inflexional even though the surface curvature is convex. The diffusion term is

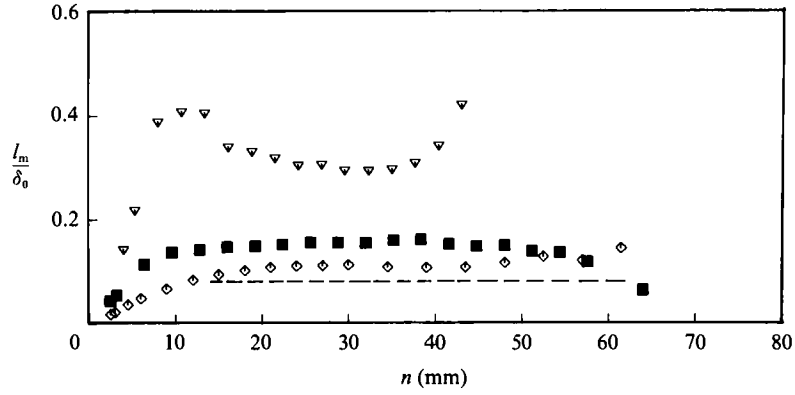

FIGURE 8. Prandtl's mixing length distributions around the concave bend. Foot of the hill: ◇, 897 mm; concave bend: ■, 1015 mm; exit: ▽, 1183 mm; consensus value in the outer region of flate plate boundary layer.

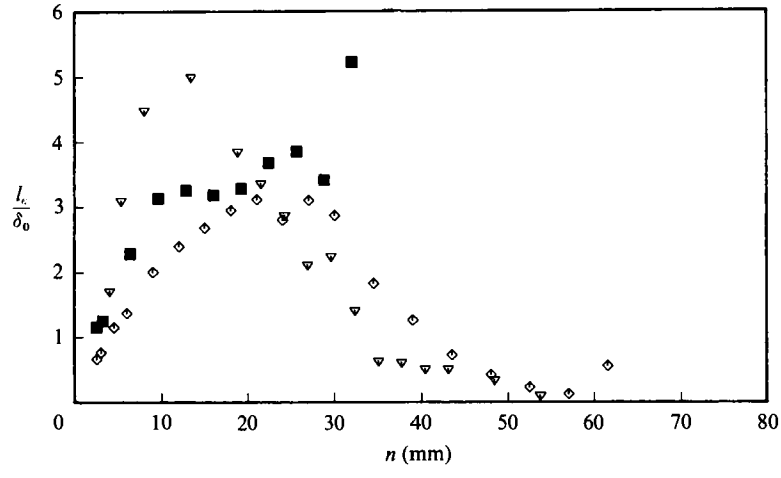

FIGURE 9. Dissipation lengthscale ($\overline{q^2}^{\frac{3}{2}}/\epsilon$) distributions around the concave bend. (For symbols refer to figure 8.)

approximately equal to the advection term below $n/\delta = 0.5$, while above this point diffusion balances dissipation, which has again become finite at the exit. In contrast, mean transport is roughly equal to turbulent transport all across the layer. Interestingly, the values of the pressure–strain term at the exit reduce to less than half of those in the bend, similar to the behaviour of the generation term. This is due to the decrease in the basic strain rate at the exit and suggests the pressure–strain redistribution term is dominated by the rapid part. Unlike the situation in the concave bend, here the model of Zeman & Jensen (1987) gives amazingly good agreement with experimental data.

The effect of curvature is also seen in the distribution of the lengthscales. Prandtl's mixing length, l_m, and the dissipation lengthscale, $L_\epsilon (= (\overline{q^2})^{\frac{3}{2}}/\epsilon)$, are shown in figures 8 and 9. Both lengthscales are equal to each other if *production = dissipation*. Hence the difference in their magnitudes in the concave bend is due to lack of energy equilibrium. The increase in both lengthscales in the bend is consistent with the sense of curvature (destabilizing). However, the increase in the bend persists at the exit demonstrating the lag effect to changes in the extra strain rate. The lag was found

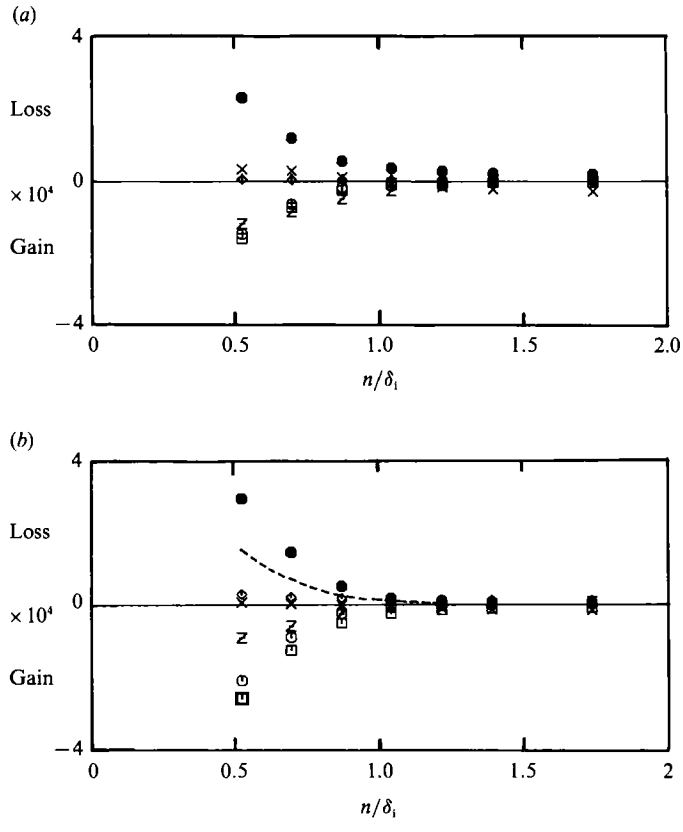

FIGURE 10. (a) Turbulent energy balance in the internal boundary layer on the windward side (s = 1469 mm). For legend refer to figure 5(a). (b) Primary shear stress balance in the internal boundary layer on the windward side (s = 1469 mm). For legend refer to figure 5(b).

to be of the order of 10δ as in the case of Smits *et al.* (1979). Using the analogy between buoyancy and curvature, Bradshaw (1969) proposed a correction for the basic flat-plate boundary-layer lengthscale, l_0, as a function of curvature Richardson number, R_i, so that $l/l_0 = 1-\alpha R_i$, with $\alpha = 2$ for concave curvature and $\alpha = 3$ for convex curvature. Here $R_i = 2S^*/(1+S^*)$, where S^* is the ratio of curvature production to the shear production (figure 4), and it is also called the 'stability parameter'. [Note that Galperin & Mellor (1989) call R_r the stability parameter where R_r is defined by the ratio of the extra strains introduced by curvature to the basic mean strain, $(\partial U/\partial n - U/r)$. Thus, $R_r = 2S^*/(1-S^*) = R_i/(1-R_i)$.] The two-fold increase in the mixing length in the bend with respect to that in the leading-edge flat-plate boundary layer is in agreement with that predicted by the above formula. The agreement for dissipation lengthscale is not so good if we have to use the above formula with the mixing length replaced by the dissipation lengthscale; the increase relative to the flat plate value is three fold in the middle of the layer. The above formula is not applicable to the exit region since the fairly thin-shear-layer approximation is strongly violated there (figure 4). In BSJ1, it was reported that the Reynolds stresses (velocity scales) changed all across the layer rather than changes being confined to the inner region as might be expected in pressure gradients. To the thin-shear-layer approximation, the effect of pressure gradients on the outer region lengthscales is usually negligible. When the thin-shear-layer approximation is

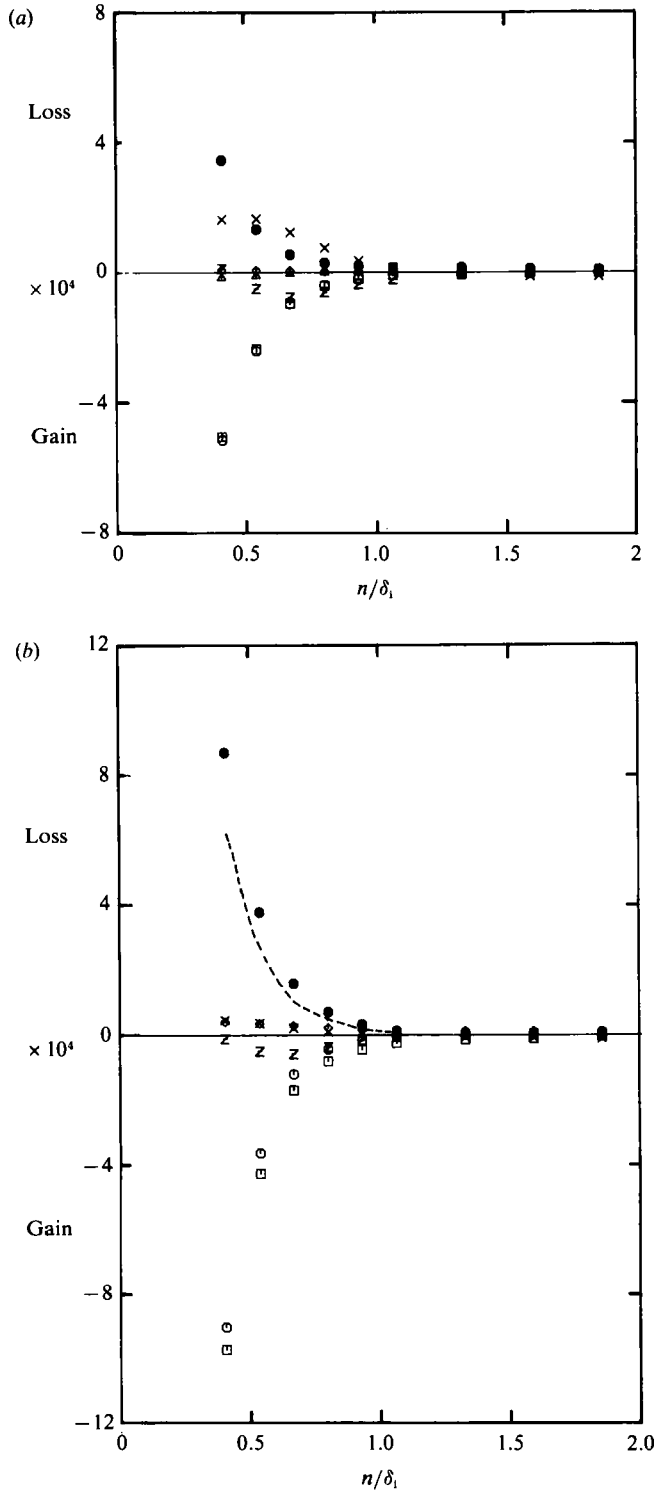

FIGURE 11. (*a*) Turbulent kinetic energy balance in the internal boundary layer at the summit (s = 1665 mm). For legend refer to figure 5(*a*). (*b*). Primary shear stress balance in the internal boundary layer at the summit (s = 1665 mm). For legend refer to figure 5(*b*).

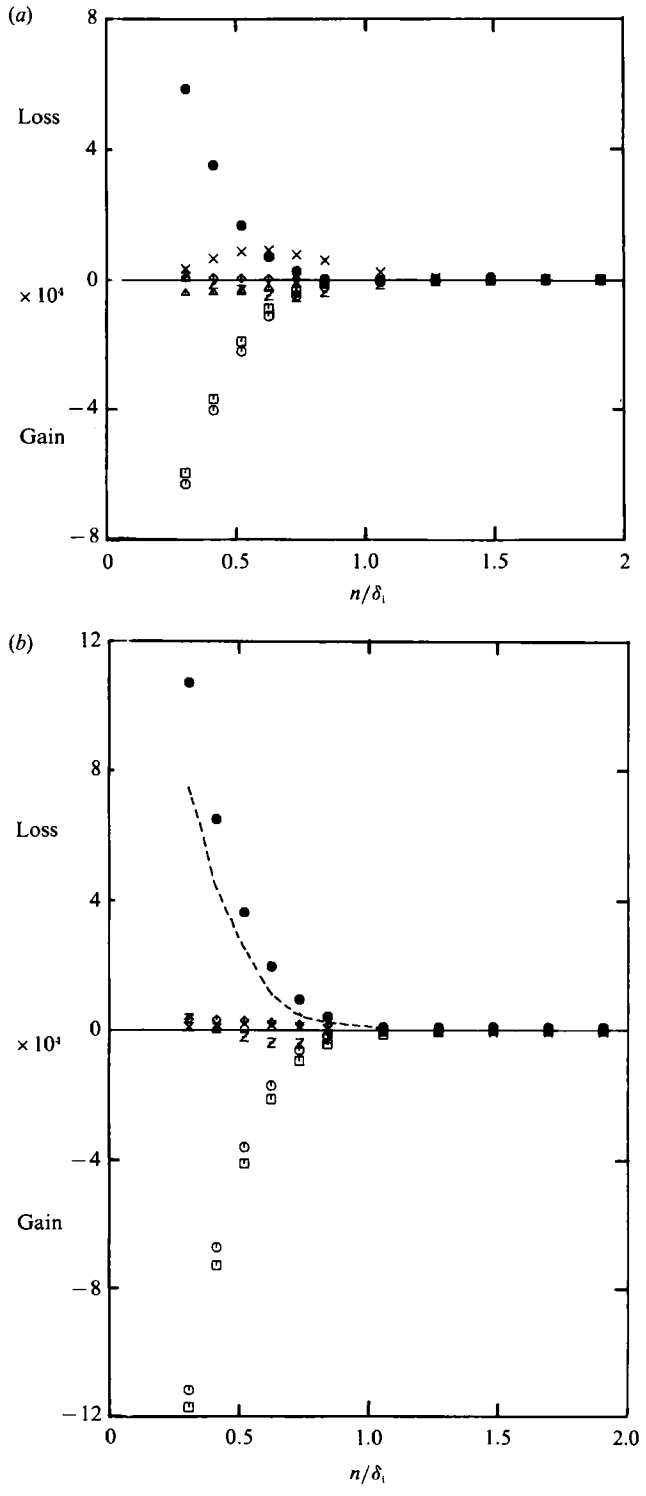

FIGURE 12. (a) Turbulent kinetic energy balance in the internal boundary layer on the lee side (s = 1862 mm). For legend refer to figure 5(a). (b) Primary shear stress balance in the internal boundary layer on the lee side (s = 1862 mm). For legend refer to figure 5(b).

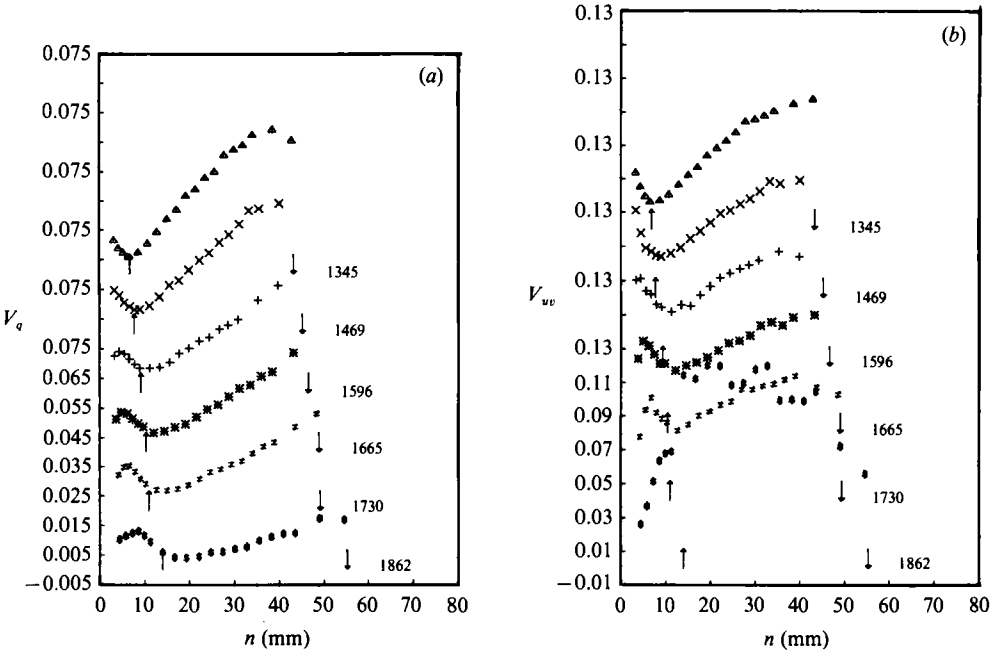

FIGURE 13. Profiles of transport velocities (*a*) Turbulent kinetic energy, V_q. (*b*) Primary shear stress, V_{uv} (for symbols refer to figure 2(*a*) and note shift in the ordinate scale).

violated, we are not sure of the mechanism by which the acceleration influences the lengthscales.

3.2. *Internal boundary layer*

The energy and the shear stress budgets in the internal boundary layer are shown in figures 10, 11 and 12 for locations on the windward side, at the summit and for the leeward side, respectively. Note that no measurements were made in the wall or inner region of the internal boundary layer since this region is too small for the cross-wire probe to access. In BSJ1, pressure gradient effects were shown to dominate this inner region and therefore streamline curvature effects are expected to be important only away from the wall. However, both normal stress production and curvature production are negligible except close to the edge of the internal boundary layer, where shear production is also small. Nevertheless, the curvature contribution to the shear stress is identifiable as a small fraction of the total generation in the shear stress budget. The slight increase in the normal stress production is expected as the internal boundary layer approaches the separation point. The internal boundary layer is not in energy equilibrium since both turbulent diffusion and advection are significant in the outer region. The outer region gains energy and shear stress through turbulent diffusion and turbulent transport respectively as indicated by the positive sign of the turbulence transport velocities V_q and V_{uv} shown in figure 13 ($V_q = \overline{q^2 v}/\overline{q^2}$, $V_{uv} = \overline{uv^2}/\overline{uv}$). The positive sign for the transport velocities in the external layer indicates there is no transfer of energy and shear stress from it into the internal layer. The pressure–strain redistribution due to Zeman & Jensen's model predicts the experimental observations fairly well (figure 12*b*).

The mixing length distributions across the internal boundary layer are shown in figure 14. The stabilizing curvature reduces the lengthscale in the outer region

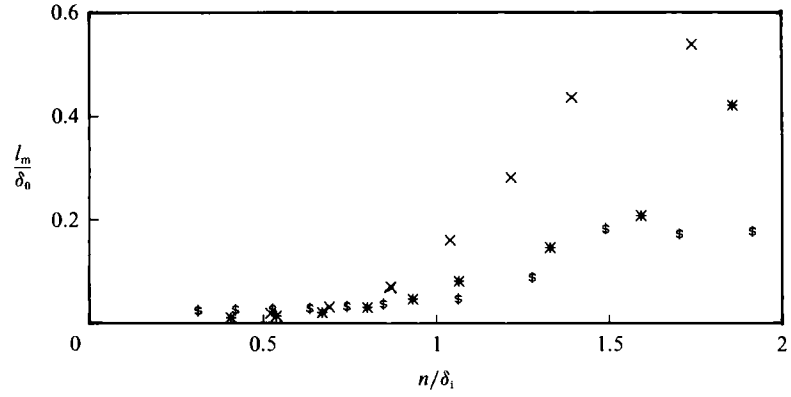

FIGURE 14. Prandtl's mixing length distributions in the internal boundary layer. Windward side: ×, 1469 mm; summit: ∗, 1665 mm; lee side: $, 1862 mm.

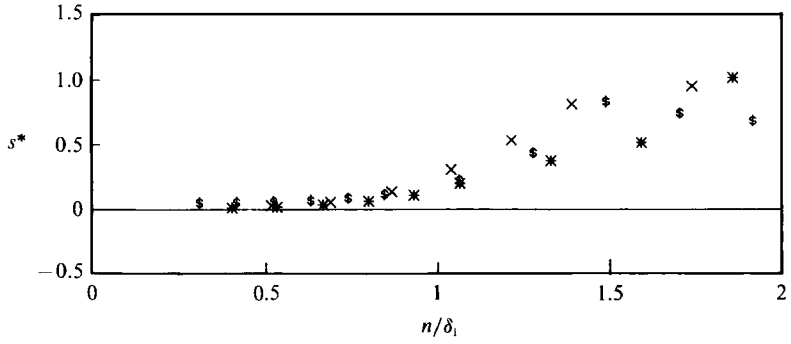

FIGURE 15. Profiles of the 'stability' parameter in the internal boundary layer. (For symbols refer to figure 14).

($n/\delta_i > 0.2$) as expected. If the mixing length is non-dimensionalized with respect to δ_i, it can be seen that the distributions inside the internal boundary layer are approximately the same as that reported by Muck *et al.* (1985) in a mildly curved convex wall boundary layer, and the distribution is expected to follow $l = \kappa n$ (κ is the Kármán constant) close to the wall. The reduction in the lengthscale is only significant in the outer twenty per cent of the internal boundary layer, where the effects of curvature are expected to be dominant. The correction to the mixing length for convex curvature recommended by Bradshaw (1969) is $l/l_0 = 1-3R_i$, where R_i was deduced from the distribution of S^* shown in figure 15. The magnitude of the mixing length is approximately the same as that given by Bradshaw's correction. The magnitude of the stability parameter, S^*, is less than 0.01 in the internal boundary layer, suggesting that the effect of streamline convex curvature is 'mild', and the thin-shear-layer approximation is obeyed. To this approximation, streamwise pressure gradient is well known to affect the flow (momentum and turbulence) only in the inner region leaving the outer flow unaffected, as shown in BSJ1. In contrast, a mild streamline curvature affects the flow only at distances far away from the wall such as in the outer or wake region as shown above. [Gibson (1988) suggests that the law of the wall for both velocity and temperature is modified by curvature. This is not found in the results presented in BSJ1.] The influence of the two extra strain rates on these two regions (inner and outer) does not appear to

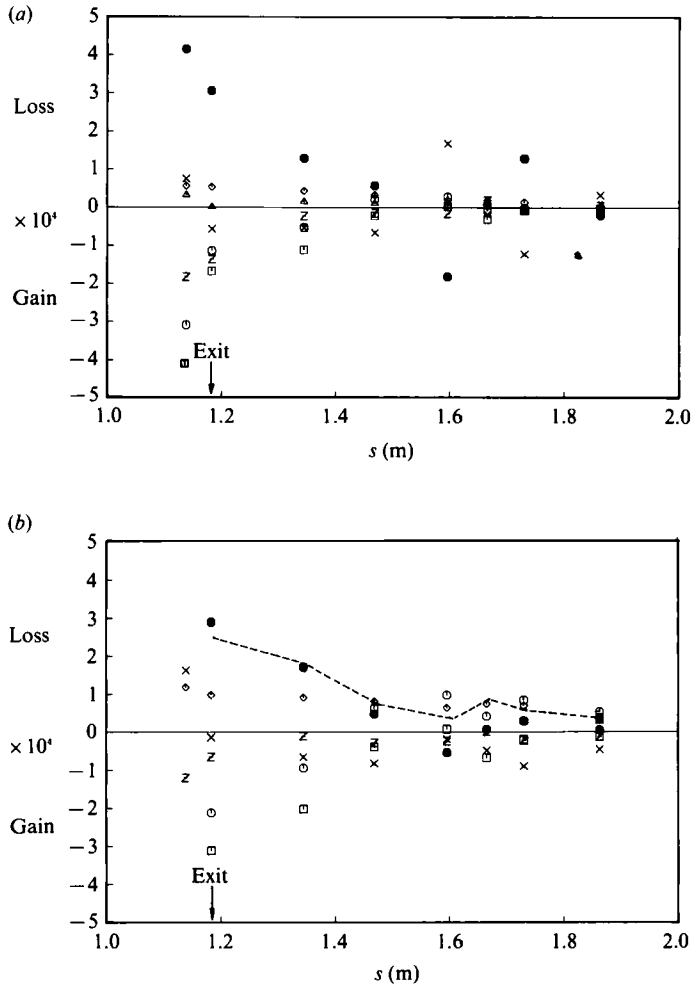

FIGURE 16. (*a*) Turbulent kinetic energy balance in the middle of the external layer. For legend refer to figure 5(*a*). (*b*) Primary shear stress balance in the middle of the external layer. For legend refer to figure 5(*b*).

overlap in the present results. This suggests that the interaction between the streamwise pressure gradient and mild streamline curvature is weak under a thin-shear-layer approximation.

3.3. *External layer*

In BSJ1, it was shown that the external layer behaves as an isolated free turbulent flow. This view is further supported here by the observation that the total production and total generation terms are zero in the external layer (figures 10, 11 and 12), and therefore the decay of turbulence with downstream distance is expected to be hastened by convex streamline curvature. Note that the rate of decrease of $\overline{q^2}$ with streamwise distance is slower than that of $-\overline{uv}$ (figure 2). The terms in (1) and (2) in the middle of the external layer, $\frac{1}{2}(\delta-\delta_1)$, are given as a function of streamwise distance in figure 16. The middle of the external layer corresponds approximately to the point where the triple product profiles in the external layer have maxima. The loss of energy and shear stress due to the curvature terms is significant because they oppose the shear terms initially. After about eight boundary-layer thicknesses downstream

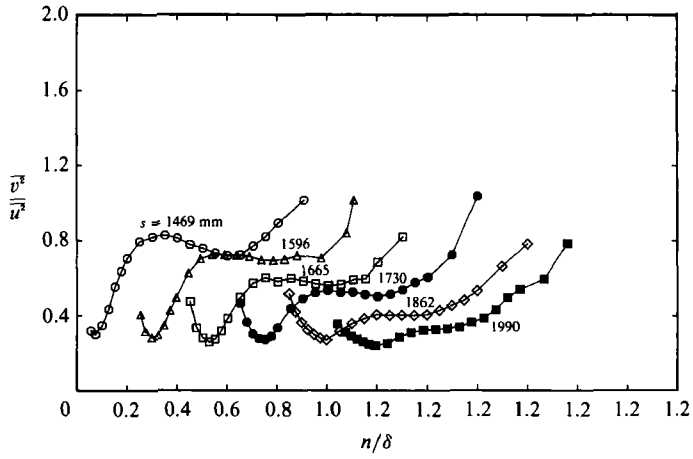

FIGURE 17. Profiles of *anisotropy* parameter, $\overline{v^2}/\overline{u^2}$, over the convex curvature region. (Note the shift in the abscissa scale.)

of the exit, the curvature and shear terms are of the same order. The acceleration does not directly contribute to the downstream decay of the energy since the normal stress production is negligibly small. Note that in the presence of curvature the turbulent diffusion and the turbulent transport processes rapidly fall to zero. This finding supports the earlier work by Muck *et al.* (1985), Ramaprian & Shivaprasad (1978), and Gibson *et al.* (1984) on the inhibiting effect of convex curvature on transport processes. This effect is also clearly evident from the profiles of transport velocities of $\overline{q^2}$ and $-\overline{uv}$ given in figure 13. The role of curvature on the shear stress decay can be clearly seen as the curvature generation term opposes the shear generation term and hence the total generation. The decay of the redistribution terms is correctly predicted by the hill-flow model of Zeman & Jensen (1987). Turbulent transport terms respond more quickly than the other terms. Gillis & Johnston (1983) found their zero pressure gradient curved external layer (the region between the knee point and the local free stream) to be isotropic in character, i.e. $\overline{u^2} = \overline{v^2} = \overline{w^2}$ and $-\overline{uv} = 0$. However, when streamwise pressure gradients are present such as in the present case, the external flow tends to become more and more anisotropic, as shown in figure 17. The declining trend in the plateau level of the anisotropy ratio suggest that $\overline{v^2}$ decays faster than $\overline{u^2}$.

4. Conclusions

The experimental results obtained in a turbulent flow over a curved hill described by BSJ1 are analysed in terms of the transport equations for the turbulent kinetic energy and the primary shear stress. The influence of streamline curvature and streamwise pressure gradients are recognized through certain terms containing the respective extra strain rates in the transport equations. The source terms due to streamline curvature relative to that due to basic shear imply that the behaviour of the primary shear stress depends on the anisotropy parameter, $\overline{u^2}/\overline{v^2}$ as well as the curvature extra strain rate. Streamwise pressure gradient does not appear to affect the shear stress directly, while its influence on the turbulent kinetic energy arises through the normal stress production term containing the extra strain rate due to acceleration.

The profiles of the triple products presented in this paper exhibit 'knee' points and

this is consistent with the fact established in Part 1 that the upwind boundary-layer structure bifurcates into an internal boundary layer and an external free turbulent flow. Both production of turbulent kinetic energy and generation of shear stress are zero in the external layer supporting the description of the external turbulent flow as being an 'isolated' or 'free'.

The extra strain rates due to concave streamline curvature and a favourable streamwise pressure gradient attain values which are about 20 % of basic shear in the bend. Consequently, even the fairly thin-shear-layer approximation breaks down. The profiles of turbulent kinetic energy exhibit little change in the outer layer as against the expected increase due to the destabilizing streamline curvature. This is due to the interaction between the streamwise pressure gradient and streamline curvature, in that the significant size of the normal stress production term counteracts the curvature production. In contrast, curvature-induced generation of shear stress augments the total generation. The increase in shear stress in the bend is genuinely due to the curvature extra strain rate since in the bend the anisotropy parameter decreases from its upstream level. The condition of energy equilibrium in the concave bend implies that the pressure fluctuations are significant. The lengthscales were found to increase under the influence of concave streamline curvature.

At the exit, the extra strain rates overwhelm the basic shear and as a result, even the fairly thin-shear-layer approximation breaks down. Both total production and total generation decrease greatly owing to a decrease in the basic strain rate rather than the curvature and pressure gradient extra strain rates. The pressure–strain redistribution term behaves in a similar manner to the generation term suggesting that the mean strain-rate dependent rapid part plays a major role.

In the region of prolonged convex curvature, the ratios of the extra strain rates to basic shear are about 0.01 suggesting a mild influence of streamline curvature and streamwise pressure gradient, and the internal boundary layer satisfies the thin-shear-layer approximation. The changes observed in the turbulence in the inner and outer regions of the internal boundary layer are found to be consistent with that expected of streamwise pressure gradient and convex streamline curvature, respectively. This in turn suggests that the interaction between the streamwise pressure gradient and streamline curvature is weak inside the internal boundary layer. Reduction of lengthscales owing to convex curvature was observed.

In the external layer, where the source terms of the transport equations are zero, turbulent diffusion of turbulent kinetic energy and turbulent transport of the shear stress were found to decrease under the influence of convex curvature. The turbulence in the external layer was found to be anisotropic, unlike the isotropic character observed by Gillis & Johnston (1983), in their curved external flow with zero pressure gradient. The pressure–strain redistribution term inferred from the present experimental data was found to agree well with the model of Zeman & Jensen (1987) everywhere, except in the concave bend. The changes in Prandtl's mixing length are well predicted by the simple formula of Bradshaw (1969) in the hill flow.

The financial support of the Australian Research Grants Scheme is gratefully acknowledged. Professor B. Galperin's comments on an earlier draft are also acknowledged with thanks. We are indebted to Professor Bradshaw for his criticism.

REFERENCES

BARLOW, R. S. & JOHNSTON, J. P. 1988 *J. Fluid Mech.* **191**, 137.

BASKARAN, V., SMITS, A. J. & JOUBERT, P. N. 1987 *J. Fluid Mech.* **182**, 47.

BRADSHAW, P. 1967 *J. Fluid Mech.* **30**, 241.

BRADSHAW, P. 1969 *J. Fluid Mech.* **36**, 177.

BRADSHAW, P. 1973 Effects of streamline curvature on turbulent flow. *AGARDograph* 169.

BRADSHAW, P. & FERRIS, D. H. 1965 The response of a retarded equilibrium turbulent boundary layer to the sudden removal of pressure gradient. *NPL Aero. Rep.* 1145, NPL, Teddington, England.

BRADSHAW, P. & UNSWORTH, K. 1974 An improved FORTRAN program for the Bradshaw–Ferris–Atwell method of calculating turbulent shear layers. *IC Aero. Rep.* 74-02.

CASTRO, I. P. & BRADSHAW, P. 1976 *J. Fluid Mech.* **73**, 265.

GALPERIN, B. & MELLOR, G. L. 1989 The effects of streamline curvature and spanwise rotation on turbulent boundary layers, submitted for publication.

GIBSON, M. M. 1988 *Zoran Zaric Memorial International Seminar on Near-Wall Turbulence*, Dubrovnik, Yugoslavia.

GIBSON, M. M. & RODI, W. 1981 *J. Fluid Mech.* **103**, 161.

GIBSON, M. M. & VERRIOPOULOS, C. A. 1984 *Exps Fluids* **2**, 25.

GIBSON, M. M., VERRIOPOULOS, C. A. & VLACHOS, N. S. 1984 *Exps Fluids* **2**, 17.

GILLIS, J. C. & JOHNSTON, J. P. 1983 *J. Fluid Mech.* **135**, 123.

HUNT, I. A. & JOUBERT, P. N. 1979 *J. Fluid Mech.* **91**, 633.

HOFFMANN, P. M., MUCK, K. C. & BRADSHAW, P. 1985 *J. Fluid Mech.* **161**, 371.

JACKSON, P. S. & HUNT, J. C. R. 1975 *Q. J. R. Met. Soc.* **101**, 929.

KOYAMA, H. 1983 *Proc. 4th Symp. on Turbulent Shear Flows, University of Karlsruhe, Karlsruhe, Germany*, p. 6.32.

MORTON, B. R. 1984 *Geophys. Astrophys. Fluid Dyn.* **98**, 277.

MUCK, K. C., HOFFMANN, P. H. & BRADSHAW, P. 1985 *J. Fluid Mech.* **161**, 347.

NAKAYAMA, A. 1987 *J. Fluid Mech.* **175**, 215.

PRABHU, A. & SUNDARASIVA RAO, B. N. 1981 Turbulent boundary layers in a longitudinally curved stream. *Rep.* 81 FM10. IISc, Bangalore, India.

RAMAPRIAN, B. R. & SHIVAPRASAD, B. G. 1978 *J. Fluid Mech.* **85**, 273.

RAMJEE, V., TULAPURKARA, E. G. & RAJASEKAR, R. 1988 *AIAA J.* **26** (8), 948.

SAVILL, A. M. 1983 in *Structure of Complex Turbulent Shear Flow* (ed. R. Dumas & L. Fulachier). Springer.

SMITS, A. J., YOUNG, S. T. B. & BRADSHAW, P. 1979 *J. Fluid Mech.* **94**, 209.

SO, R. M. C. & MELLOR, G. L. 1972 An experimental investigation of turbulent boundary layers along curved surfaces. *NASA CR*-1940.

TOWNSEND, A. A. 1961 *J. Fluid Mech.* **11**, 97.

WOOD, D. H. & BRADSHAW, P. 1984 *J. Fluid Mech.* **139**, 347.

ZEMAN, O. & JENSEN, N. O. 1987 *Q. J. R. Met. Soc.* **113**, 55.